Applied Catalysis A: General 469 (2014) 410–418

Contents lists available at ScienceDirect

Applied Catalysis A: General

journal homepage: www.elsevier.com/locate/apcata

Gas-phase, catalytic hydrodeoxygenation of propanoic acid, over supported group VIII noble metals: Metal and support effects

Yuliana K. Lugo-José, John R. Monnier, Christopher T. Williams*

Department of Chemical Engineering, University of South Carolina, Columbia 29208, SC, USA

ARTICLE INFO

Article history:
Received 15 July 2013
Received in revised form 9 October 2013
Accepted 14 October 2013
Available online xxx

Keywords:
Biomass
Hydrodeoxygenation
Decarbonylation
Decarboxylation
Hydrogenation
Propanoic acid
Palladium catalyst

ABSTRACT

The catalytic, gas-phase hydrodeoxygenation (HDO) of propanoic acid (PAc) over supported group VIII noble metals (M = Pd, Pt, Rh, Ru, Ni) was studied at 1 atm and 200-400 °C. The activity and selectivity as a function of the reaction temperature was investigated. The reaction activity based on the TOF follows the order: Pd > Ru > Pt > Rh > Ni. The reaction over Pd, Pt and Rh catalysts proceeds mainly via decarbonylation (DCN) and decarboxylation (DCX) pathways at each reaction temperature. For Ru and Ni catalysts, while decarbonylation and decarboxylation pathways were predominant at lower temperatures (e.g., 200–250 °C), at higher temperatures (>300 °C) the formation of diethyl ketone was observed. Additionally, the kinetics of Pd over different supports (carbon, SiO_2 and TiO_2) were examined. The activity based on the TOF decreases in the following order: Pd/SiO_2 > Pd/TiO_2 > Pd/C. The reaction orders in acid and H_2 were found to be approximately 0.5 and zero, respectively, regardless of the support. The apparent activation energies studied in a temperature range of 200–240 °C, were 16.7 ± 0.6, 19.3 ± 1.6 and 11.7 ± 0.7 kcal/mole for Pd/C, Pd/TiO_2 and Pd/SiO_2 catalysts, respectively. The selectivity for Pd/C and Pd/SiO_2 indicated mainly decarbonylation/decarboxylation and hydrogenation reaction pathways. In contrast, Pd/TiO_2 at low temperatures (200 °C) could generate decarbonylation and esterification products.

1. Introduction

The demand of energy is increasing constantly and the United States is dependent on foreign sources for about half of its fuel consumption [1]. The combustion of fossil fuels releases carbon dioxide, a major greenhouse gas, into the atmosphere contributing to the problem of global warming. This factor, along with the increasing demand for fossil fuels coupled with the decreasing availability of those resources, has prompted a move towards alternative energy production and utilization [2,3]. New research efforts promise to bring advances in a variety of areas, and biomass conversion to fuels and chemicals will play a critical role in the future.

Industrial processes for converting biomass into biofuels include gasification to syngas (leading to liquid fuels through FT synthesis), pyrolysis to produce bio-oil, and hydroprocessing to remove oxygen functionality [4–6]. During these processes, carbon dioxide is released as well; however, the emission gases are balanced largely by the carbon dioxide that is captured during the growth of the biomass, depending upon how much energy was used to grow, harvest and process the fuel [7]. Feedstocks derived from lignocellulosic substances contain great amounts of oxygen such that the C:O ratio approaches unity. However, the fuel and chemical products derived from such feedstocks must have an oxygen content less than about 5.0% to be commercially viable [8,9]. Heterogeneous, catalytic deoxygenation (including hydrodeoxygenation) is one of the most promising processes for generating hydrocarbon fuels from biomass. During hydrodeoxygenation (HDO), hydrogen is co-fed with the reactant to facilitate hydrogenolysis (HYS) and hydrogenation reactions required for the removal of oxygen.

During the 1980s, Maier et al. studied the gas-phase decarboxylation of short chain carboxylic acids to hydrocarbons using Ni and Pd catalysts [10]. However, most of this work focused on C–C bond scission rather than removal or hydrogenation of the C=O bond. Since then, increasing amounts of research have been conducted in the area of biomass-derived platform molecules such as organic acids and esters (e.g., palmitic, oleic and stearic acid, ethyl stearate and tristearine) via decarboxylation and hydrogenation reactions on monometallic and bimetallic catalysts [11–28]. For example, Murzin and co-workers have focused on biomass- derived, liquid-phase hydrogenation on supported palladium catalysts [29], while Resasco and Lobban reported the direct conversion of triglycerides to olefins and paraffins over Pt/Al_2O_3, Pt/SiO_2, and $PtSnK/SiO_2$ catalysts [30]. Additionally, Kozhevnikov et al. recently reported studies on heteropoly acid and bifunctional metal-loaded heteropoly acid catalysts for the deoxygenation of PAc [31].

* Corresponding author. Tel.: +1 803 777 0143; fax: +1 803 777 8265.
E-mail address: willia84@cec.sc.edu (C.T. Williams).

0926-860X/$ – see front matter © 2013 Elsevier B.V. All rights reserved.
http://dx.doi.org/10.1016/j.apcata.2013.10.025

Table 1
Physical and chemical properties of M/SiO_2.

Metal loading (wt%)	Catalyst Mx/SiO_2	Calcination temp. (°C)	Reduction temp. (°C) 100% H_2	Dispersion (%) O_2–H_2 titr.	Particle diameter (nm)
1.1	Pd	300	350	3.9	31.4
4.0	Pd*	–	350	55.0	2.0
2.1	Pt	–	300	11.7	9.7
2.2	Rh	–	300	21.0	5.3
1.6	Ru	300	300	11.7	11.4
1.8	Ni	450	450	4.8	22.6

* Pd/SiO_2 synthesized by SEA.

Eqs. (1)–(6) illustrate the hydrogenation, decarbonylation, and decarboxylation pathways proposed for the HDO of organic acids and esters. In addition, the CO_2 and CO products from the decarboxylation (DCX) and decarbonylation (DCN) routes can undergo further reaction through water–gas shift and methanation, consuming large amount of H_2.

$$\text{Hydrogenation}: \quad R_1 - COO - R_2 + 4H_2 \leftrightarrow R_1 - CH_3 + R_2 - H + 2H_2O \tag{1}$$

$$R - COOH + 3H_2 \leftrightarrow R - CH_3 + 2H_2O \tag{2}$$

$$\text{Decarbonylation}: \quad R_1 - COO - R_2 + 2H_2 \leftrightarrow R_1 - H + R_2 - H + CO + H_2O \tag{3}$$

$$R - COOH + H_2 \leftrightarrow R - H + CO + H_2O \tag{4}$$

$$\text{Decarboxylation}: \quad R_1 - COO - R_2 + H_2 \leftrightarrow R_1 - H + R_2 - H + CO_2 \tag{5}$$

$$R - COOH \leftrightarrow R - H + CO_2 \tag{6}$$

The present work aims to explore the catalytic chemistry of the HDO of PAc (a model compound for aliphatic organic acids) over supported group VIII noble metal catalysts. The monometallic catalysts have been selected based on their potential to catalyze different bond breaking events relevant to the above reactions. The catalysts include Pd, Pt, Ru, Rh and Ni supported on SiO_2. Additionally, Pd was screened on different supports (i.e. carbon, SiO_2, and TiO_2) to investigate the influence of the support material on activity, selectivity and activation energy. These studies provide insight on the different reaction pathways to form paraffins/olefins or oxygenated products from biomass derived organic acids.

2. Experimental

2.1. Catalyst synthesis (M/SiO_2)

For the screening reaction on M/SiO_2 (M = Pd, Ru, Ni), the catalysts were synthesized by incipient wetness utilizing aqueous solutions of the following metal salts: palladium nitrate hydrate ($Pd(NO_3)_2{\cdot}xH_2O$, 99.9 Sigma-Aldrich), ruthenium nitrosyl nitrate ($Ru(III)(NO)(NO_3)_3$, 31.3% min Alfa Aesar) and nickel perchlorate hexahydrate ($Ni(II)(ClO_4)_2{\cdot}6H_2O$, 99.99% Alfa Aesar). The SiO_2 support (Silica Star, S_{BET} = 100 m^2/g) and the commercial catalysts of 2.14 wt% Pt and 2.06 wt% Rh over SiO_2, were obtained from BASF. In addition, a 4.0 wt% Pd catalyst with a different SiO_2 support (Aerosil 300, S_{BET} = 330 m^2/g, Evonik) was synthesized by strong electrostatic adsorption (SEA), where the pH of the metal salt complex solution (200 ppm of $[Pd(NH_3)_4]^{2+}Cl_2$, 99.9% Sigma Aldrich) was controlled based on the PZC of the SiO_2 [32,33]. Once the pH of the solution is acquired, the support was impregnated and shaken for 1 h. After the final pH was obtained, the difference (ΔpH) indicated that a strong electrostatic interaction between the metal precursor and the –OH group on the support took place, allowing a controlled impregnation with highly dispersed metal precursors [34–36]. The catalysts prepared by SEA or incipient wetness were dried overnight at 70 °C, followed by calcination in air and reduction with 100% H_2 at their respective temperatures for 2 h (see Table 1). The exception was the 4 wt% Pd/SiO_2, which was not subjected to a calcination step due to the fact that the 1.1 wt% Pd/SiO_2 catalyst exhibited very large particle size. The commercial catalysts were already prepared, and therefore it was decided that no calcination step was required.

2.2. Catalyst synthesis (Pd/X)

Three different palladium catalysts were investigated for the detailed kinetics of the HDO of PAc: 4.0 wt% Pd/SiO_2 (Aerosil 300, S_{BET} = 330 m^2/g, Evonik), 5.0 wt% Pd/C (CP-97, S_{BET} = 615 m^2/g, commercial BASF catalyst) and 2.3 wt% Pd/TiO_2 (TiO_2, S_{BET} = 46.1 m^2/g, Evonik). The Pd/SiO_2 and Pd/TiO_2 catalysts were synthesized by SEA, while the commercial Pd/C was supplied by BASF and followed the same procedure described in the previous section.

3. Pulsed H_2 chemisorption

The metal dispersions of the catalysts were determined by pulsed hydrogen titration of oxygen pre-covered sites using a Micromeritics 2920 AutoChem II Analyzer. Prior to the analysis, the catalysts (0.1–0.2 g) were reduced in flowing 100% H_2 for 2 h, followed by purging with Ar for 2 h to remove any physisorbed hydrogen. After cooling to 40 °C in flowing Ar, the catalysts were exposed to 10% O_2/He for 30 min followed by purging with Ar (30 min). Titration with pulses of 10% H_2/Ar was then employed until no further H_2 uptake occurred. This method was applied for Pd, Pt, and Rh based catalysts. For Ru and Ni, a modified hydrogen chemisorption method was implemented. The sample experienced the same pretreatment described previously; however, no H_2-chemisorption at 40 °C was done. After being exposed to argon, the sample was heated up to 100 °C by temperature programmed oxidation, following by flushing with argon for 30 min. Then, the sample temperature was raised up to 225 °C and exposed to 10% H_2/Ar. This titration temperature was confirmed based on the results of temperature programmed oxidation/reduction described in the Supplemental Information.

3.1. Catalyst evaluation

The activity and selectivity of each catalyst was measured for the HDO of PAc. The experiments were carried out in a single pass, packed bed, plug flow reactor system. The catalysts were reduced in-situ at temperatures ranging from 200 to 400 °C at a total flow of 50 sccm H_2 for 2 h at 1 atm pressure. The reduction temperature was chosen depending on the different reduction treatments required for each metal (Table 1). The feed stream for the screening experiments consisted of 1.0% PAc (Alfa Aesar, 99%) and 20% H_2,

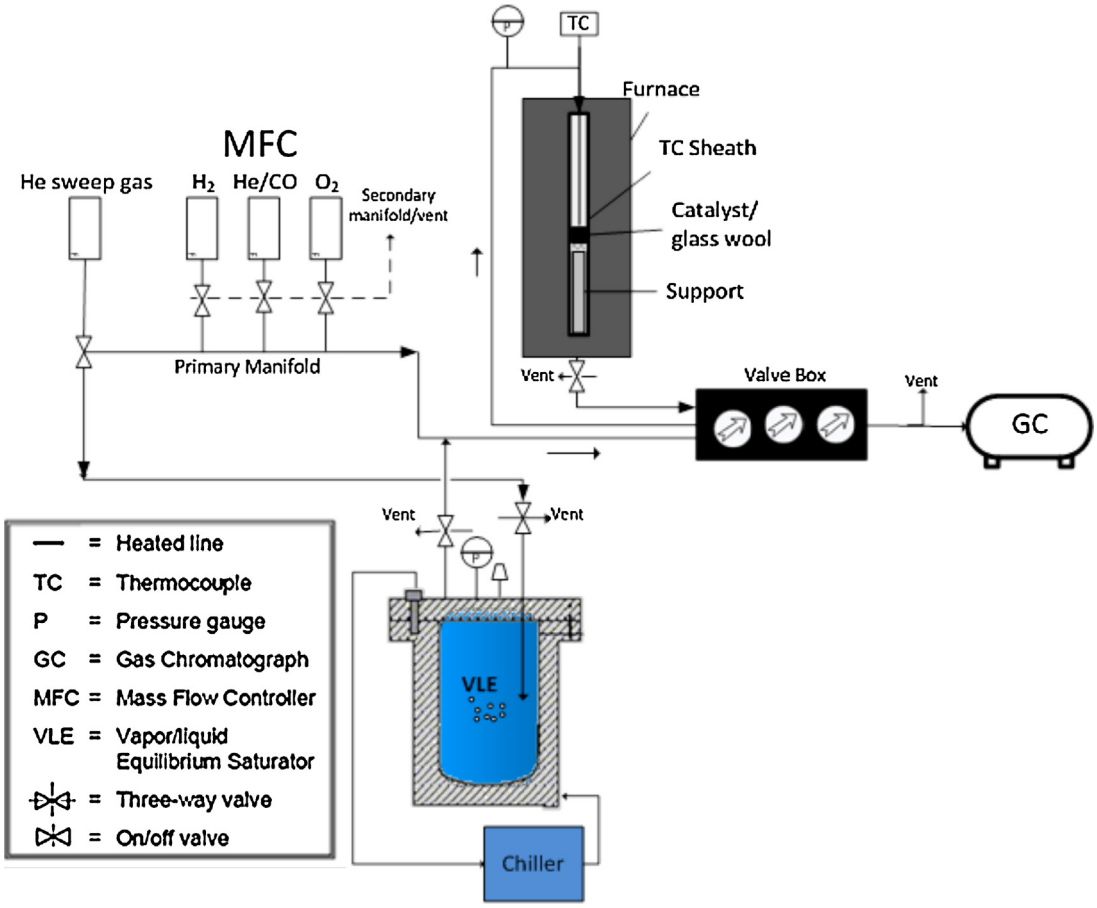

Fig. 1. Schematic of the vapor phase continuous plug-flow reactor system.

balances He. For the kinetic experiments, PAc and H_2 concentrations ranged from $X_{PAc} \sim 0.0020–0.017$ and $X_{H_2} \sim 0.20–0.99$. Fig. 1 shows a schematic of the plug flow reactor system including the Brooks mass flow controllers (MFC), vapor–liquid equilibrium saturator (VLE), switching valve box, and the GC inlet. PAc (Alfa Aesar, 97%) was used as received. The gas feed and product lines (going through the valve and reactor) were heated >100 °C, to prevent acid and product condensation. Reaction products were analyzed by an on-line Hewlett-Packard 5890 gas chromatograph equipped with two Poraplot Q capillary columns; one was linked to a flame ionization detector (FID) for analysis of organic products and unreacted PAc, while the second column was connected to a thermal conductivity detector for analysis of permanent gases such as CO and CO_2. Carbon monoxide hydrogenation experiments were also conducted for two M/SiO_2 (M = Ru, Ni) catalysts to explore their degree of methanation activity. The concentration of carbon monoxide was maintained at 1.0% to simulate what might be encountered during the HDO reaction based on the amount of PAc that was being fed. The conversion and selectivity for a given catalyst was defined according to the following equations:

$$\text{Conversion} = \left(\frac{PAc_{in} - PAc_{out}}{PAc_{in}}\right) \times 100$$

$$\text{Selectivity} = \left(\frac{P_i/\lambda_i}{\sum_i^n P_i/\lambda_i}\right) \times 100$$

where PAc_{in} and PAc_{out} denote the concentrations of PAc before and after the reaction, and λ_i, P_i are the stoichiometric factor and product concentration, respectively.

4. Results and discussion

4.1. Hydrodeoxygenation of PAc over M/SiO_2: Effect of reaction temperature

The effect of reaction temperature on the hydrodeoxygenation activity of PAc was investigated over the range 200–400 °C. The reactions are classified, based on the formation of main products, as decarbonylation/decarboxylation for hydrocarbon products and hydrogenation and ketonization (for oxygenated products). Prior to examining the HDO of PAc on various SiO_2-supported group VIII noble metals, the activity and selectivity over two different SiO_2 supports were explored. Fig. 2a and 2b shows the conversion and selectivity as a function of temperature for Silica Star and Aerosil 300. These supports were capable of catalyzing the ketonization reaction due to the acid properties of the silica surface [37]. Reaction over Silica Star resulted in the formation of diethyl ketone (DEK) at temperatures above 300 °C around 92% selectivity. The remaining 8% of products consisted of small amounts of ethane and propionaldehyde. The reaction over SiO_2 Aerosil 300, resulted primarily in the formation of DEK (73% selective), but also ethylene (27% selective) at temperatures above 350 °C, suggesting the Aerosil 300 has lower surface acidity. Pestman and co-workers have reported reactions of carboxylic acids over metal oxides (i.e., Al_2O_3, Fe_2O_3, SiO_2) [38,39]. According to their work, a bimolecular ketonization reaction was observed that produced DEK along with

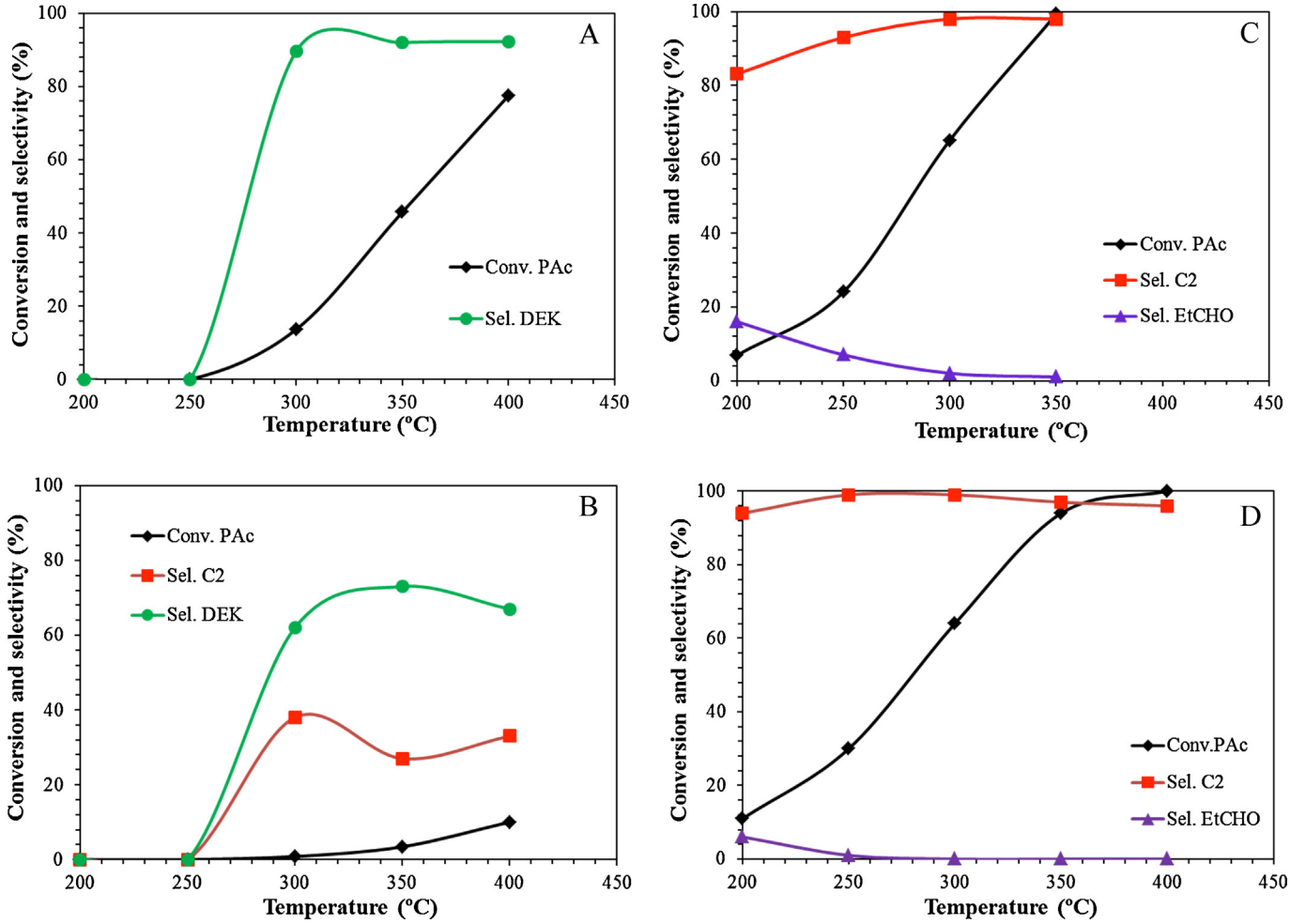

Fig. 2. Conversion and selectivity for (a) Silica Star and (b) Aerosil 300 SiO_2 supports; (c) 1.1 wt% Pd/Silica Star and (d) 4.0 wt% Pd/Aerosil 300. C2 denotes the sum of ethylene and ethane. EtCHO and DEK refer to propionaldehyde and diethyl ketone, respectively. Mass of catalyst (100–300 mg); feed composition 1% PAc, 20% H_2, balance He. Total flow rates for 1.1 wt% and 4 wt% Pd/SiO_2 were 50 and 200 sccm, respectively.

CO_2 and water. According to their findings, for metal oxide surfaces with high metal-oxygen bond strength (i.e. SiO_2, TiO_2), the reactant required at least one reactive α-hydrogen atom to form a ketene-like intermediate which subsequently reacted with an adsorbed carboxylate species (from a second molecule of adsorbed carboxylic acid) to form the ketone [40].

The physical and chemical properties (i.e. dispersion and particle size) for M/SiO_2 catalysts are summarized in Table 1. Catalyst evaluation data for 1.1 wt% Pd/SiO_2 (incipient wetness) and 4.0 wt% Pd/SiO_2 (SEA) catalysts are summarized in Fig. 2c and d. For 1.1 wt% Pd/SiO_2, complete conversion is reached at 350 °C with 98% selectivity to ethane. Conversely, at lower temperatures of 200 °C, the product distribution is mainly ethane (83%) and some propionaldehyde (17%), a deoxygenation product formed by C–OH cleavage. Thus, even at 200 °C, the reaction proceeds mainly through decarbonylation and hydrogenation pathways supported by CO formation. The reaction result is in agreement with previous work conducted by Lamb et al., where the liquid-phase HDO of carboxylic acids over Pd/SiO_2 catalyst occurred mainly via decarbonylation at 300 °C [41]. The reaction over 4 wt% Pd/SiO_2 shows 94% conversion at 350 °C with 97% and 3% selectivities toward ethane and methane, respectively. At lower temperatures (200 °C), the product distribution is mainly ethane (94%), with lower production of propionaldehyde (6% selective). The different selectivities with respect to propionaldehyde formation at 200 °C could be attributed to a combination of particle and support effects. The 2 nm particles present for the 4 wt% catalyst have a significantly larger fraction of step and kink sites than the 31 nm particle for the 1.1 wt% catalyst (Table 1), which contain primarily low index (1 1 1) and (1 0 0) crystal faces. Another explanation may be the different degrees of acidity for the two SiO_2 supports, as indicated by the data in Fig. 2a and b. Such possible effects are currently under further investigation.

Given that DEK was formed on both the Silica Star and (to a much lesser extent) Aerosil 300 supports at temperatures of 300 °C and above, it was important to consider whether this species could undergo reaction to form ethane and/or propionaldehyde at these temperatures on the supported Pd catalyst. Thus, the activity of DEK on 1.1 wt% Pd/SiO_2 (incipient wetness) catalyst was explored to address this issue. Hydrodeoxygenation of DEK was conducted between 200 and 400 °C using 1.0% DEK, 20% H_2, and the balance He. The results confirmed negligible activity (<3% conversion) only by 400 °C, indicating that the observed product formation over the Pd catalyst during HDO of PAc was not proceeding through this pathway on the support surface.

Catalyst performances for 2.1 wt% Pt and 2.0 wt% Rh on SiO_2 show selectivity only towards hydrocarbons. The results indicate mainly decarbonylation based on the observation of CO production as opposed to CO_2. Fig. 3(a) and (b) shows the conversion and corresponding selectivities to C_2 and C_3 hydrocarbons for the Pt and Rh catalysts, respectively, as a function of temperature. Measurable PAc conversions were detected at temperatures above 200 °C

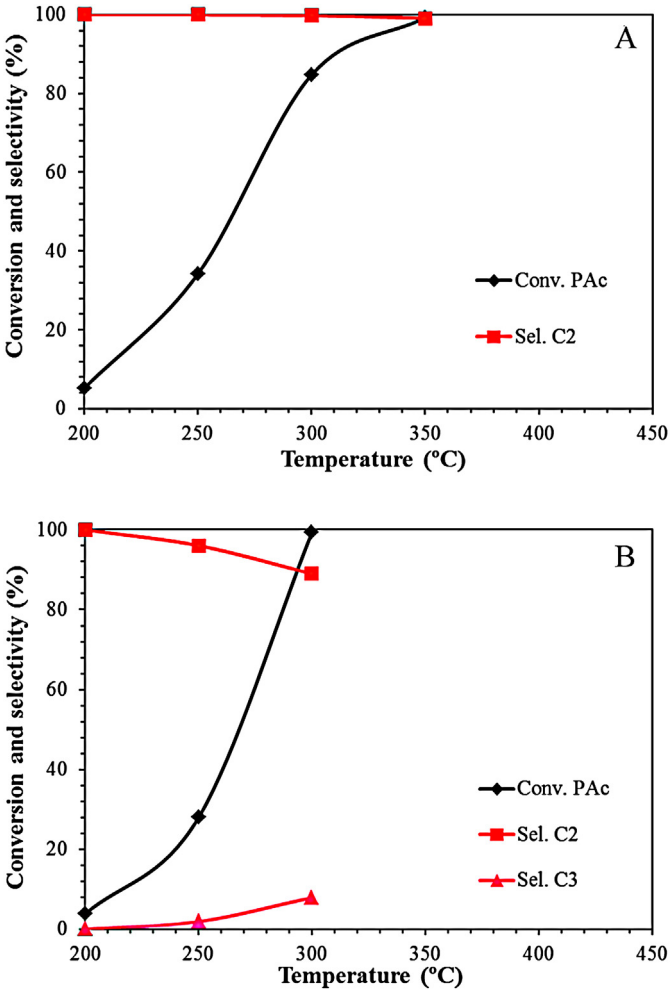

Fig. 3. Conversion and selectivity for (a) Pt and (b) Rh supported on SiO_2 Star. C2 and C3 denote ethane and propane, respectively. Mass of catalyst (200–300 mg); feed composition 1% PAc, 20% H_2, balance He; total flow rate 50 sccm.

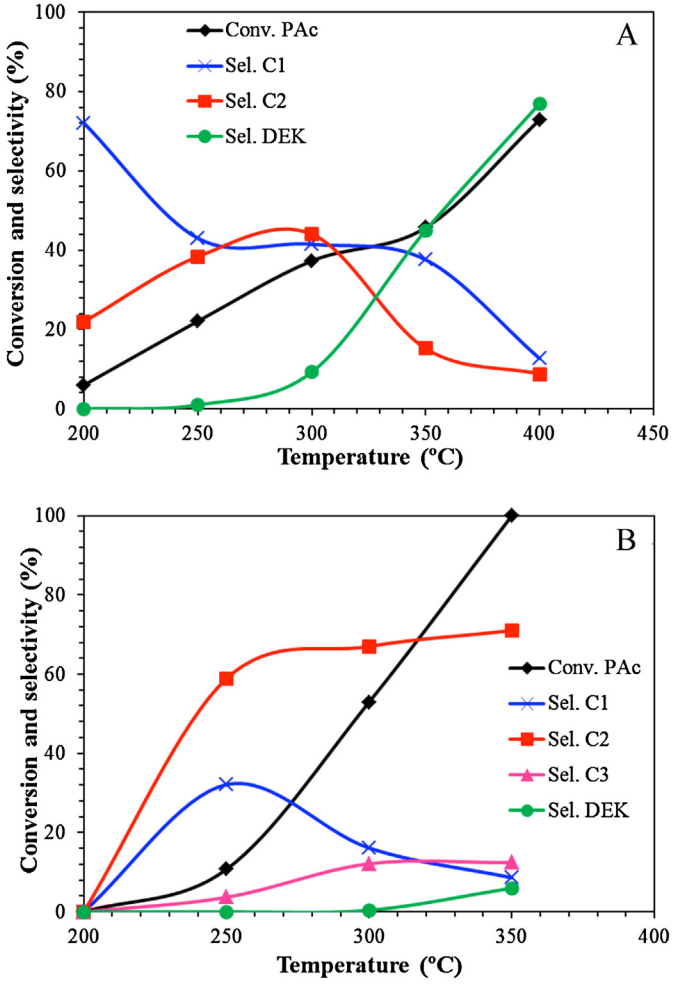

Fig. 4. Conversion and selectivity for (a) Ru and (b) Ni over SiO_2 Star. C2 denotes as the sum of ethylene and ethane C3 denote as propane. EtCHO and DEK denote propionaldehyde and diethyl-ketone respectively. Mass of catalyst (200–300 mg); feed composition 1% PAc, 20% H_2, balance He; total flow rate 50 sccm.

and the conversion was complete at temperatures above 300 °C for Rh and above 350 °C for Pt. At complete conversion, Pt/SiO_2 shows 100% selectivity to ethane, while Rh/SiO_2 mainly shows selectivity to ethane (89%) and some propane (10%), revealing that some hydrodeoxygenation/hydrogenation is occurring for the formation of propane.

For the reactions with Ru and Ni supported on SiO_2, at high conversion levels, both oxygenated compounds and cracking products are observed. Fig. 4(a) shows that the selectivity for Ru/SiO_2 at 200 °C, is mainly towards methane (72%), ethane (22%) and small traces of propane and butane (6%). As the temperature approaches to 350 °C, the selectivity changes toward DEK (45%), suggesting PAc interaction at the surface the support. At this temperature, considerable amounts of methane were formed (38% selectivity). Therefore, methanation experiments were conducted to verify whether the catalyst can produce methane by CO hydrogenation at similar temperatures. Based on these methanation experiments (see Supporting information Table S1), no substantial amount of methane is produced over the temperature range 200–400 °C. Therefore, methane is considered to be produced via the cracking of PAc and/or ethane.

For Ni/SiO_2 (Fig. 4(b)), very low activity (<1% conversion) is observed at 200 °C, although at 250 °C, conversion increases to 11% to form mainly methane (32%) and ethane (59%). However, as the temperature is raised to 350 °C, the conversion reaches 100% and the product distribution is mainly ethane (71%) and propane (12%), indicative of decarbonylation and hydrodeoxygenation/hydrogenation. At 350 °C, the catalyst shows methane (9%) and DEK (6%) formation. This methane is formed by CO hydrogenation, as a similar yield of methane is obtained during direct methanation of CO at similar temperature (see Supporting information, Table S2).

In addition to selectivity pattern studies at variable temperatures, experiments were conducted at low conversion at 200 °C and 1 atm for all the M/SiO_2 catalysts. Table 2 summarizes the reaction rates in μmol product formed/min g_{cat} and turnover frequencies (TOF, molecules $site^{-1} min^{-1}$). The non-rate performance parameters such as conversion, selectivities towards oxygenated and nonoxygenated hydrocarbon products, and the carbon balance, which is the ratio of carbon atoms in the reactor outlet to carbon atoms in the reactor inlet. The reaction rates were restricted to differential conversion (<10%), and followed the order: Pd > Rh ~ Pt > Ru > Ni. According to the rates per g catalyst, 4.0 wt% Pd/SiO_2 was approximately 25 times higher than for 1.1 wt% Pd/SiO_2. However, when activities are expressed as turn over frequencies (activity per surface site of Pd), the orders are reversed, with the lower dispersion 1.1 wt% Pd catalyst being more active by a factor of 2. While there may be some support acidity effects, the most likely explanation is that the nature and distribution of the exposed Pd sites are different in these catalysts due to different particle sizes. Overall, the TOF values followed a similar trend as reaction rates with the order: Pd > Ru > Pt > Rh > Ni. The work

Table 2
Kinetic data for the screened catalysts in the HDO of PAc at 200 °C and 1 atm. ~1.0% PAc, 20% H_2/He, catalyst mass 100–300 mg, total flow 50 sccm. Pd* was measured at a total flow 200 sccm.

Metal loading (wt%)	Catalyst Mx/SiO_2	Rate (μmol/min g_{cat})	TOF (min^{-1})	Conv. (%)	Select. to organic products (%)	Select. to hydrocarbons (%)	C atoms outlet/ C atoms inlet
1.1	Pd	2.57	0.64	7.0	17	83	1.0
4.0	Pd*	69.1	0.32	11.0	6	94	1.0
2.1	Pt	1.60	0.12	5.0	0	100	1.0
2.1	Rh	1.89	0.05	4.0	0	100	0.9
1.6	Ru	4.55	0.24	6.0	0	100	1.0
1.8	Ni	0.13	0.009	1.0	0	100	–

conducted by Kozhevnikov et al. on the deoxygenation of PAc, suggested comparable activity trends when Pd and Pt are compared (i.e., Pd > Pt) [31]. The Ni/SiO_2 catalyst was the least active at 200 °C, consistent with previous investigations that gave similarly poor activities for nickel-based catalysts for the HDO of carboxylic acids [42,43].

4.2. Catalytic evaluation of palladium on various supports

In addition to examining the catalytic performance of various group VIII noble metals over SiO_2, the influence of different supports on the activity and selectivity of Pd for the hydrodeoxygenation of PAc was explored. Three different supported Pd catalysts were evaluated for detailed kinetics: 5.0 wt% Pd/C, 4.0 wt% Pd/SiO_2 and 2.3 wt% Pd/TiO_2. Prior to these studies, the performances of the carbon and TiO_2 supports alone were examined, as shown in Fig. 5(a–b). For carbon, no significant activity was observed until 350 °C, where at 10% conversion, small amounts of ethane (78% selectivity) were formed; the remaining products consist of C_2 and C_3 hydrocarbons and propionaldehyde. In contrast, for TiO_2 at 300 °C conversion was 20% and DEK was produced at 100% selectivity. This indicates a strong interaction between the acid and the support that lead to ketonization catalyzed by acidic sites on TiO_2.

Fig. 6(a) for 5.0 wt% Pd/C shows very high selectivity (100%) at 200 °C and 91% selective at >350 °C, towards ethane with balance CH_4 over the entire temperature range of 200–350 °C, producing mainly CO. The results are in agreement with work of Murzin and co-workers on the continuous liquid-phase deoxygenation of lauric acid over 5 wt% Pd/C [44]. They reported an activity of 44% conversion and 98% selectivity to undecane at 300 °C. Both studies indicate that decarbonylation and/or decarboxylation is/are the main reaction pathways. In contrast, for 2.3 wt% Pd/TiO_2 (Fig. 6(b)) the reaction temperature has a significant effect on product distribution. At 200 °C, the selectivity is primarily towards oxygenated compounds (15% propanol, 59% *n*-propyl-propionate) and some ethane (23%). As the temperature increases, the selectivity towards ethane is increased with no evidence of *n*-propyl-propionate formation above 300 °C, which indicates that decarbonylation is favored above this temperature, due to the formation of CO, verified by gaseous products analyses generated by the TCD at the different temperatures studied. At complete conversion (300 °C), the reaction was selective toward ethane (90%) with balance propanol (10%) due to decarbonylation and hydrodeoxygenation respectively.

Table 3 summarizes the physical properties (i.e., metal dispersion, particle diameter) and catalyst evaluation results for these three catalysts. The TOF values decrease in the following order: Pd/SiO_2 > Pd/TiO_2 > Pd/C. The Pd/TiO_2 and Pd/SiO_2 catalysts exhibit TOF values 20 and 30 times higher, respectively, than Pd/C, which can be attributed to a combination of particle size [45,46] and/or support effects. It is difficult to assign the higher activities to support effects alone, since TiO_2 and SiO_2 have markedly different physiochemical properties, yet both are much more active than the carbon-supported Pd catalyst. These issues are currently under further investigation in our laboratory.

A series of plausible reaction pathways (Scheme 1) have been developed to better understand the performance of these catalysts. For Pd/C at 200–250 °C, the reaction pathway is more consistent with decarbonylation, based on the simultaneous formation of ethane and CO. At higher temperatures (>300 °C), CO_2 is produced, which could be due to decarboxylation, but also the water–gas shift (WGS) reaction. Therefore, the WGS equilibrium constants of K_{eq} ~ 38.1, 19.9 and 11.5 at 300, 350 and 400 °C [47], respectively, were used to calculate the maximum amount of CO_2 that could be produced by WGS reactions between 350-400 °C. Results showed that WGS could account for only < 5% of the CO_2 actually observed. Consequently, at 350–400 °C the reaction proceeds mainly via decarbonylation and decarboxylation, with negligible

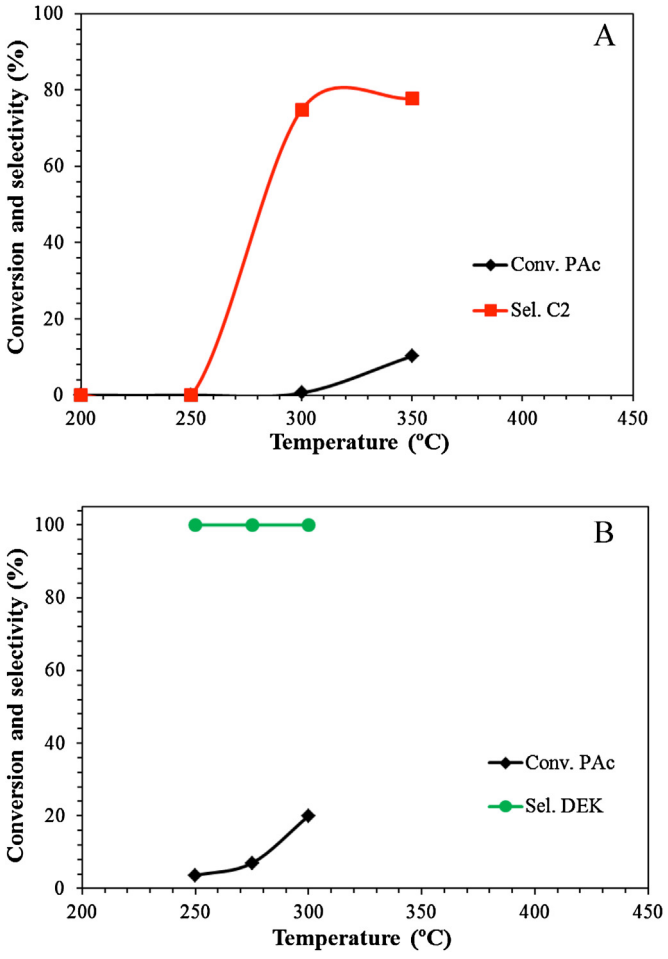

Fig. 5. Conversion and selectivity for (a) carbon and (b) TiO_2. C2 denotes as the sum of ethylene and ethane. DEK denote as diethyl-ketone. Mass of catalyst (200–300 mg); feed composition 1% PAc, 20% H_2, balance He; total flow rate 50 sccm.

Table 3
Kinetic data for the HDO of PAc over supported Pd catalyst. Reaction conditions: 200 °C and 1 atm, X_{PAc} = 0.01, 20% H_2/balance He, catalyst weight: Pd/C—200 mg, Pd/SiO_2 and Pd/TiO_2—100 mg.

Metal loading (wt%)	Catalyst	Disp. (%)	Particle size d_{nm}	Conv. (%)	Sel. oxygenate (%)	Sel. non-oxygenate (%)	C atoms outlet/ C atoms inlet	TOF (min^{-1})
5.0	Pd/C	16.9	6.8	2.0	0	100	1.0	0.01
4.0	Pd/SiO_2	55.2	2.0	4.0	6	94	1.0	0.32
2.3	Pd/TiO_2	27.3	4.1	3.3	42	58	1.4	0.20

WGS. However, at 300 °C, the amount of CO_2 that could be formed based on WGS equilibrium would be equivalent to ~50% of the CO_2 that was actually observed. Therefore, it is possible that some of the CO_2 formed at 300 °C was from WGS, with the remaining amount produced from decarboxylation.

For Pd/SiO_2, similar results are observed. The reaction pathways consist mainly of decarbonylation and hydrogenation steps. PAc is primarily decarbonylated to produce ethane and CO, although the formation of small amounts of propionaldehyde indicates hydrogenation of PAc also occurs, especially at lower temperatures (200–250 °C). In contrast, Pd/TiO_2 exhibits different reaction pathways. At low temperatures (~200 °C), the formation of propanol and *n*-propyl propionate is observed. At temperatures >225 °C, ethane, CO and CO_2 are observed, indicating decarbonylation and decarboxylation. The results are consistent with previous studies for the hydrogenation of carboxylic acids over Pt/TiO_2, where it was claimed that oxygen vacancies were generated on the oxide support from the hydrogen spillover of Pd during reduction [50]. Hence, a plausible reaction pathway over Pd/TiO_2 could be the generation of oxygen vacancies at the interface of the catalyst, which in turn weakens the C=O bond of PAc to favor the formation of propanol and water. Esterification of propanol with PAc can then occur to form *n*-propyl propionate. At higher temperatures, however, decarbonylation of PAc to form ethane and CO becomes the predominant reaction pathway.

4.3. Kinetics of palladium on various supports

The reaction rates of the three catalysts can be expressed as power rate law equations, $r = A\exp\left(-\frac{E_a}{RT}\right)\prod_{i=1}^{n}P_i^{xi}$, where A is the pre-exponential factor, E_a is the activation energy, P_i is the partial pressure of species i, and x_i is the reaction order of species i. The apparent reaction order is obtained from the slope of ln reaction rate vs. ln mole fractions of PAc and H_2 (X_{PAc} and X_{H2}, respectively). Fig. 7 shows the plots for 5.0 wt% Pd/C, 4.0 wt% Pd/SiO_2 and 2.3 wt% Pd/TiO_2. For all catalysts, the reaction orders in PAc and H_2 are approximately 0.5 and 0, respectively, over the range of concentrations examined. It can be seen based on the formation of CO, that decarbonylation is the dominant deoxygenation pathway under these conditions, which is consistent with the computational studies of Heyden [47] for the DCX and DCN of PAc on Pd(1 1 1) model surfaces. Heyden's computations indicated the most kinetically-favorable pathway was decarbonylation and the rate controlling steps included dehydroxylation of PAc (C–OH bond cleavage) to produce propanoyl (CH_3CH_2CO), which was followed by α carbon dehydrogenation to form C_2 hydrocarbons. Thus, the rate determining step is dependent on the capacity to remove the hydrocarbon pool (CH_3CH_x) from the surface, which could explain why the reaction order for PAc was less than first order. For H_2, the reaction order of zero implies a high coverage of hydrogen on the Pd surface, relative to PAc reaction intermediates. Interestingly, even though Pd/SiO_2 and Pd/TiO_2 have different reaction pathways that lead to hydrogenation and esterification products such as aldehydes, alcohols and esters, the reaction orders are not affected by the supports even though the selectivity trends are significantly different.

The Arrhenius plots for each catalyst are shown in Fig. 8. Activation energy values of 16.7 ± 0.6, 19.3 ± 1.6 and 11.7 ± 0.7 kcal/mole were obtained for the Pd/C, Pd/TiO_2 and Pd/SiO_2 catalysts, respectively. The apparent activation energies were calculated based on the total consumption rates of PAc, and therefore represent an

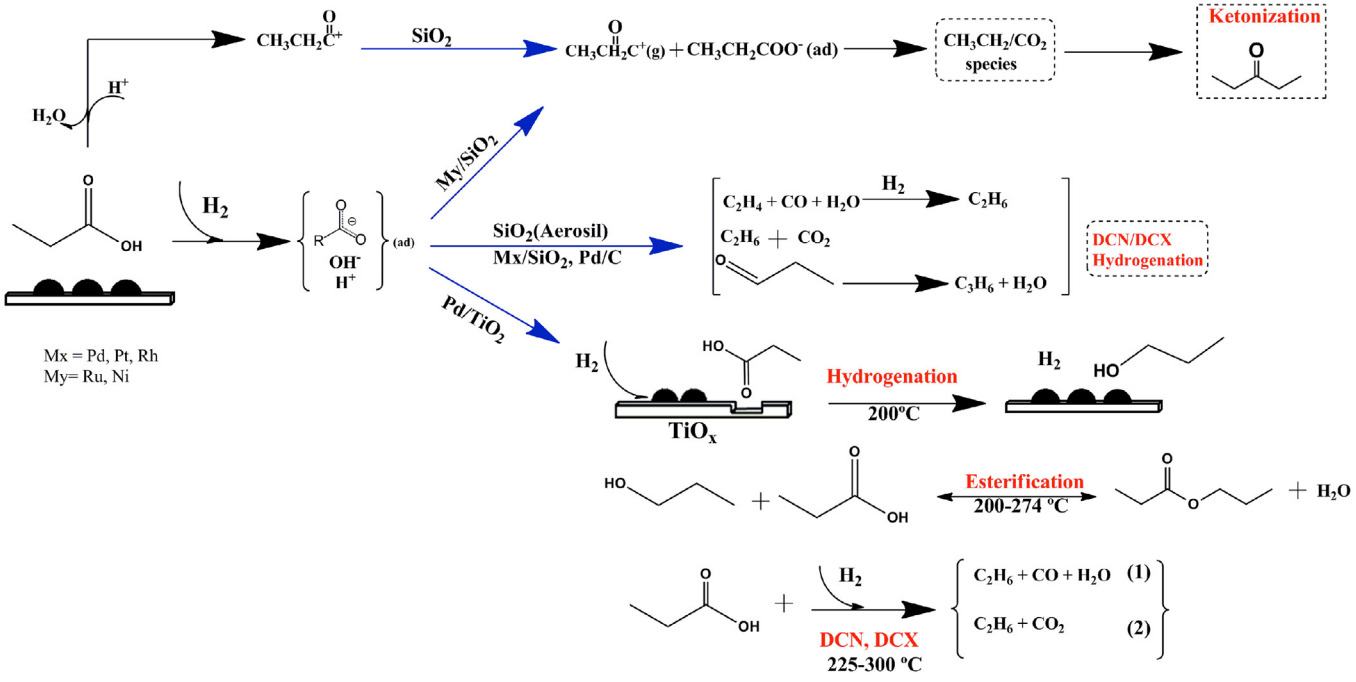

Scheme 1. Plausible reaction mechanism for the HDO of PAc over Pd over SiO_2, C and TiO_2, between 200 and 400 °C. Mx/SiO_2 (Pd, Pt, Rh), My/SiO_2 (Ru, Ni).

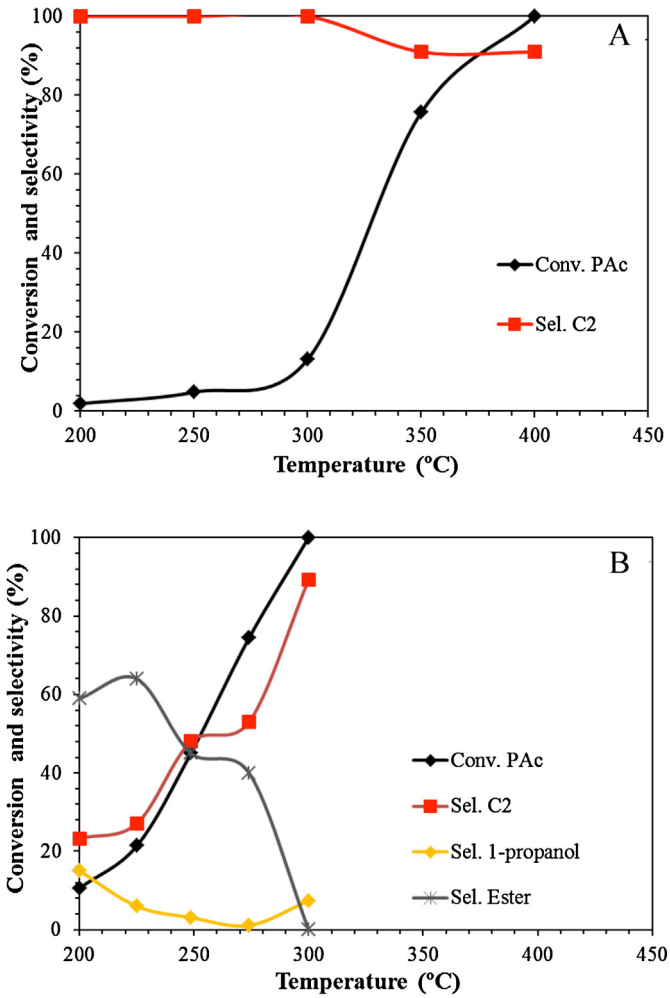

Fig. 6. Conversion and selectivity for (a) Pd/C and (b) Pd/TiO_2. C2 denotes as the sum of ethylene and ethane. Ester denotes as propyl-propionate. Mass of catalyst (100–200 mg); feed composition 1% PAc, 20% H_2, balance He; total flow rate 50 sccm.

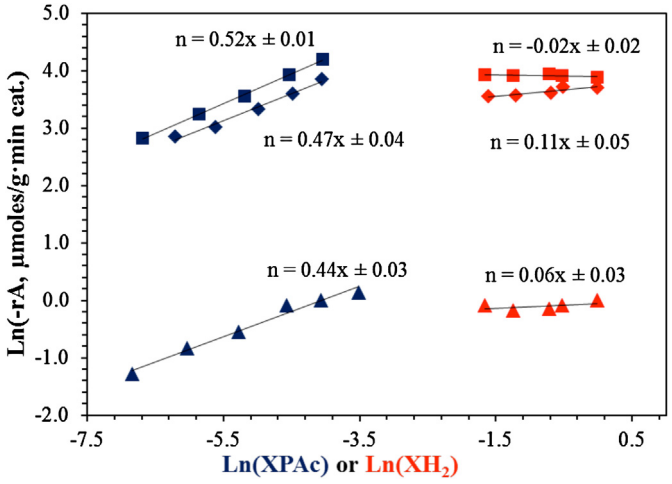

Fig. 7. Power rate law for the kinetic dependencies of PAc and H_2 for PAc conversion at 200 °C and 1 atm pressure. (■) 4.0 wt% Pd/Aerosil 300, (♦) 2.3 wt% Pd/TiO_2, (▲) 5 wt% Pd/C, reactor conditions: 20% H_2/balance, total flow: Pd/C—50 sccm, Pd/SiO_2—200 sccm, Pd/TiO_2—150 sccm. For hydrogen kinetics ~ 1.0% PAc balances He.

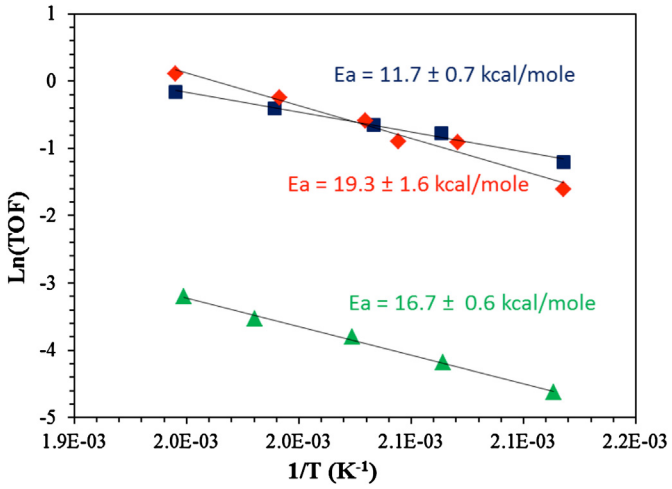

Fig. 8. Arrhenius apparent activation energies for (■) 4.0 wt% Pd/Aerosil 300, (♦) 2.3 wt% Pd/TiO_2 and (▲) 5 wt% Pd/C.

aggregate of multiple pathways. Pd/C exhibit mainly decarbonylation/decarboxylation reactions, where Pd/SiO_2 and Pd/TiO_2 exhibit hydrogenation/decarbonylation reactions. For Pd/C, the results are in general agreement with previous work [48,49], where activation energy values for the vapor-phase hydrogenation of carboxylic acids over platinum group metals ranged from 13–16 kcal/mol. In the case of Pd/SiO_2, a recent investigation [31] has reported an E_a value of 8.4 kcal/mol over the temperature range 250–300 °C, which is lower than the value reported here (11.7 kcal/mol). However, in addition to the temperature range being higher, the selectivity in the previous study was towards ethylene as opposed to ethane observed here, suggesting different mechanistic behavior.

While the lower E_a value of 11.7 kcal/mol for Pd/SiO_2 might suggest the presence of some external mass transfer limitations [50], the experiments here were conducted in the kinetic regime. This was confirmed by varying the flow rates over a range of 50–250 sccm for each catalyst to determine the minimum flow rate where the reaction rate remained constant (and thus free of external mass transfer limitations). The minimum flow rates where no external mass transport limitations were observed were found to be 50, 200 and 150 sccm for Pd/C, Pd/SiO_2 and Pd/TiO_2, respectively, and these were the flow rates used in the kinetic studies.

In addition to confirming the absence of external mass transfer limitations, intraparticle diffusion limitations could be dismissed since application of the Weisz–Prater criterion showed that the silica pore diameters were much lower than the mean free path (λ) of PAc, indicating that diffusivity was governed by Knudsen diffusion and that internal mass transport limitations were absent [51–53]. The criterion represents a useful technique, which includes parameters that can be calculated to determine if the reaction process is operating in a diffusion or reaction-limited regime. In order to determine the absence of pore diffusion limitations the following equation has to be satisfied:

$$N_{W-P} = \frac{\Re_{PAc}\rho_c R_p^2}{C_s D_{eff}} \leq 0.3 \quad (9)$$

where $\Re_{PAc}$ (moles/s g_{cat}) denotes the rate of reaction of PAc, ρ_c (g_{cat}/cm^3) is the catalyst pellet density, R_p (cm) is the radius of the particle, C_s ($moles/cm^3$) is the concentration of PAc at the surface of the catalyst (assuming that it is the same as the bulk concentration) and D_{eff} is the effective diffusion coefficient. If the support pore diameter is much less than the mean free path (λ), the diffusivity is governed by Knudsen diffusion. The criterion values for Pd over carbon, TiO_2 and SiO_2 were 4.5E − 04, 2.4E − 05 and 1.8E − 02

respectively, confirming the absence of internal mass transport limitations. Recently, Lopez-Ruiz and Davis used the same criterion for confirming the absence of internal mass transport during the decarbonylation of heptanoic acid over Pt/C [54]. Therefore, we are confident that the lower E_a value of 11.7 kcal/mol reflects the true kinetics of the reaction. The observations for the lower E_a for Pd/SiO_2 compared to Pd/TiO_2 and Pd/C might be due again to a combination of support and particle size effect, and this is currently under investigation.

5. Conclusion

In conclusion, gas-phase HDO of PAc over various supported metal catalysts has been carried out. For M/SiO_2 catalysts, the choice of group VIII noble metal has a significant effect on the selectivity, which is also significantly influenced by the temperature. At 200 °C the main reaction pathways for the HDO of PAc under the explored conditions are: (1) hydrogenation, decarbonylation and decarboxylation over Pd, Pt and Rh based catalysts, and (2) decarbonylation and methanation, followed by ketonization at high temperatures over Ru and Ni respectively. The TOF for the PAc conversion is highest over Pd-based catalysts, suggesting that this metal is the most effective for this class of reactions of the ones tested. Kinetic studies over Pd on different supports indicate that the activity (TOF) changes depending on the support, thus indicating a combination of particle size and support effects. For all Pd catalysts, the apparent reaction order with respect of PAc and hydrogen is half and zero order, respectively. These reaction orders are consistent with rate determining steps involving C–OH bond cleavage and the removal of hydrocarbon pool species (e.g., CH_3C_x) from the surface of the catalyst. These initial findings have formed the basis for more focused studies of the effect of Pd particle size on activity and the influence of adding second metal to Pd (i.e., bimetallic effects), and will be the subject of future reports.

Acknowledgments

The authors wish to thank the financial support from National Science Foundation (NSF) grant number CHE-1153012. Yuliana Lugo-José thanks the Sloan Foundation and the NSF Southeastern Alliance for Graduate Education and the Professoriate (SEAGEP) for financial support. The authors thank Professors Andreas Heyden and John R. Regalbuto from the University of South Carolina for their helpful and insightful conversations.

Appendix A. Supplementary data

Supplementary data associated with this article can be found, in the online version, at http://dx.doi.org/10.1016/j.apcata.2013.10.025.

References

[1] B. ASSOC, Annu. Energy Rev. 2010 (1949–2010) 384.
[2] S. National Academy of, E. National Academy of, M. Institute of, P. National Academies, What You Need to Know about Energy, National Academies Press, Washington, DC, 2008.
[3] D.A. Simonetti, J.A. Dumesic, Catalysis Review 51 (2009) 441–484.
[4] D.G. Lima, V.C.D. Soares, E.B. Ribeiro, D.A. Carvalho, É.C.V. Cardoso, F.C. Rassi, K.C. Mundim, J.C. Rubim, P.A.Z. Suarez, Journal of Analytical and Applied Pyrolysis 71 (2004) 987–996.
[5] A.V. Bridgwater, Chemical Engineering Journal 91 (2003) 87–102.
[6] J. Michael Robinson, C.E. Burgess, M.A. Bently, C.D. Brasher, B.O. Horne, D.M. Lillard, J.M. Macias, H.D. Mandal, S.C. Mills, K.D. O'Hara, J.T. Pon, A.F. Raigoza, E.H. Sanchez, J.S. Villarreal, Biomass and Bioenergy 26 (2004) 473–483.
[7] C. Bessou, F. Ferchaud, B. Gabrielle, B. Mary, Agronomy for sustainable development, EDP Sciences 31 (2011) 1–79.
[8] T.V. Choudhary, C.B. Phillips, Applied Catalysis A: General 397 (2011) 1–12.
[9] A.V. Bridgwater, D. Meier, D. Radlein, Organic Geochemistry 30 (1999) 1479–1493.
[10] W.F. Maier, W. Roth, I. Thies, P.V. Schleyer, Chemische Berichte/Recueil 115 (1982) 808–812.
[11] J.C. Serrano-Ruiz, A. Pineda, A.M. Balu, R. Luque, J.M. Campelo, A.A. Romero, J.M. Ramos-Fernández, Catalysis Today 195 (2012) 162–168.
[12] B.J. O'Neill, E.I. Gürbüz, J.A. Dumesic, Journal of Catalysis 290 (2012) 193–201.
[13] C.A. Henao, D. Braden, C.T. Maravelias, J.A. Dumesic, A novel catalytic strategy for the production of liquid Fuels from Ligno-cellulosic biomass, in: M.C.G.E.N. Pistikopoulos, A.C. Kokossis (Eds.), Computer Aided Chemical Engineering, Elsevier, 2011, pp. 1723–1727.
[14] R.M. West, E.L. Kunkes, D.A. Simonetti, J.A. Dumesic, Catalysis Today 147 (2009) 115–125.
[15] J.Q. Bond, D. Wang, D.M. Alonso, J.A. Dumesic, Journal of Catalysis 281 (2011) 290–299.
[16] S.G. Wettstein, J.Q. Bond, D.M. Alonso, H.N. Pham, A.K. Datye, J.A. Dumesic, Applied Catalysis B: Environmental 117–118 (2012) 321–329.
[17] E.W. Ping, J. Pierson, R. Wallace, J.T. Miller, T.F. Fuller, C.W. Jones, Applied Catalysis A: General 396 (2011) 85–90.
[18] S.J. Tauster, S.C. Fung, R.L. Garten, Journal of the American Chemical Society 100 (1978) 170–175.
[19] T.C. Chang, J.J. Chen, C.T. Yeh, Journal of Catalysis 96 (1985) 51–57.
[20] S.J. Tauster, Accounts of Chemical Research 20 (1987) 389–394.
[21] I. Simakova, O. Simakova, P. Mäki-Arvela, A. Simakov, M. Estrada, D.Y. Murzin, Applied Catalysis A: General 355 (2009) 100–108.
[22] H. Bernas, K. Eränen, I. Simakova, A.-R. Leino, K. Kordás, J. Myllyoja, P. Mäki-Arvela, T. Salmi, D.Y. Murzin, Fuel 89 (2010) 2033–2039.
[23] D.Y. Murzin, M. Snare, I. Kubickova, P. Maki-Arvela, K. Eranen, J. Warna, The Chemical Engineering Journal 134 (2007) 29–34.
[24] S. Lestari, I. Simakova, A. Tokarev, P. Mäki-Arvela, K. Eränen, D. Murzin, Catalysis Letters 122 (2008) 247–251.
[25] S. Lestari, P. Mäki-Arvela, I. Simakova, J. Beltramini, G. Lu, D. Murzin, Catalysis Letters 130 (2009) 48–51.
[26] I. Kubicková, M. Snåre, K. Eränen, P. Mäki-Arvela, D.Y. Murzin, Catalysis Today 106 (2005) 197–200.
[27] J.N. Chheda, J.A. Dumesic, Catalysis Today 123 (2007) 59–70.
[28] M. Chia, J.A. Dumesic, Chemical Communications 47 (2011) 12233–12235.
[29] S. Lestari, P.i. Mäki-Arvela, H. Bernas, O. Simakova, R. Sjöholm, J. Beltramini, G.Q.M. Lu, J. Myllyoja, I. Simakova, D.Y. Murzin, Energy & Fuels 23 (2009) 3842–3845.
[30] M. Chiappero, P.T.M. Do, S. Crossley, L.L. Lobban, D.E. Resasco, Fuel 90 (2011) 1155–1165.
[31] M.A. Alotaibi, E.F. Kozhevnikova, I.V. Kozhevnikov, Applied Catalysis A: General 447–448 (2012) 32–40.
[32] T.E. Feltes, L. Espinosa-Alonso, E.d. Smit, L. D'Souza, R.J. Meyer, B.M. Weckhuysen, J.R. Regalbuto, Journal of Catalysis 270 (2010) 95–102.
[33] R. John, Strong electrostatic adsorption of metals onto catalyst supports, in: Catalyst Preparation, CRC Press, Boca Raton, FL, 2006, pp. 297–318.
[34] S. Lambert, N. Job, L. D'Souza, M.F.R. Pereira, R. Pirard, B. Heinrichs, J.L. Figueiredo, J.-P. Pirard, J.R. Regalbuto, Journal of Catalysis 261 (2009) 23–33.
[35] L. Jiao, J.R. Regalbuto, Journal of Catalysis 260 (2008) 329–341.
[36] J.T. Miller, M. Schreier, A.J. Kropf, J.R. Regalbuto, Journal of Catalysis 225 (2004) 203–212.
[37] R.L. Augustine, Catalyst support, in: M. Dekker (Ed.), Heterogeneous catalysis for the synthetic chemist, Marcel Dekker Inc, New York, 1996, pp. 153–178.
[38] R. Pestman, R.M. Koster, A. vanDuijne, J.A.Z. Pieterse, V. Ponec, Journal of Catalysis 168 (1997) 265–272.
[39] R. Pestman, A. Vanduijne, J.A.Z. Pieterse, V. Ponec, Journal of Molecular Catalysis A: Chemical 103 (1995) 175–180.
[40] M. Renz, European Journal of Organic Chemistry (2005) 979–988.
[41] J.P. Ford, J.G. Immer, H.H. Lamb, Topics in Catalysis 55 (2012) 175–184.
[42] A.T. Madsen, E.H. Ahmed, C.H. Christensen, R. Fehrmann, A. Riisager, Fuel 90 (2011) 3433–3438.
[43] W.F. Maier, W. Roth, I. Thies, P.V.R. Schleyer, Chemische Berichte 115 (1982) 808–812.
[44] P. Mäki-Arvela, M. Snåre, K. Eränen, J. Myllyoja, D.Y. Murzin, Fuel 87 (2008) 3543–3549.
[45] R. Van Hardeveld, F. Hartog, Surface Science 15 (1969) 189–230.
[46] G.C. Bond, Surface Science 156 (1985) 966–981, Part 2.
[47] J. Lu, S. Behtash, A. Heyden, The Journal of Physical Chemistry C 116 (2012) 14328–14341.
[48] D.A. Bulushev, J.R.H. Ross, Catalysis Today 163 (2011) 42–46.
[49] W. Rachmady, M.A. Vannice, Journal of Catalysis 192 (2000) 322–334.
[50] G.W. Roberts, Chemical Reactions and Chemical Reactors, John Wiley & Sons, Hoboken, NJ, 2008.
[51] P.G. Smirniotis, Angewandte Chemie International Edition 46 (2007), 1007-1007.
[52] P.B. Weisz, C.D. Prater, Interpretation of measurements in experimental catalysis, in: V.I.K.W.G. Frankenburg, E.K. Rideal (Eds.), Advances in Catalysis, Academic Press, New York, 1954, pp. 143–196.
[53] M.E. Davis, R.J. Davis, Fundamentals of chemical reaction engineering, 1st ed. ed, McGraw-Hill, Dubuque, IA, 2002.
[54] J.A. Lopez-Ruiz, R.J. Davis, Green Chemistry (2013), Advance Article.